# COMPTEL observations of the $\gamma$-ray blazars 3C 454.3 and CTA 102 during the CGRO mission

S. Zhang[1,2], W. Collmar[2], and V. Schönfelder[2]

[1] Laboratory for Particle Astrophysics, Institute of High Energy Physics, PO Box 918-3, Beijing 100049, PR China
   e-mail: szhang@mail.ihep.ac.cn
[2] Max-Planck-Institut für extraterrestrische Physik, Postfach 1613, 85741 Garching, Germany

**ABSTRACT**

We have investigated the MeV behaviour of the $\gamma$-ray blazars 3C 454.3 and CTA 102 by analyzing all COMPTEL observations of this sky region during the complete CGRO mission. Both sources are detected by COMPTEL at the upper COMPTEL energies, although their flux estimates may be uncertain by possible minor contributions of nearby unidentified EGRET $\gamma$-ray sources. While CTA 102 was only detected at energies above 10 MeV during the early mission, 3C 454.3 is most significantly detected in the COMPTEL 3–10 MeV band in the sum of all data. Time-resolved analyses indicate a weak (near COMPTEL threshold) but likely steady 3–10 MeV emission over years, being independent of the observed time variability at energies above 100 MeV as observed by EGRET. This energy-dependent variability behaviour suggests different emission mechanisms at work in the two bands. Putting the COMPTEL fluxes in multifrequency perspective (radio to $\gamma$-rays) reveals for both sources the typical two-hump blazar spectrum, with a low-energy maximum around the IR and a high-energy maximum at MeV energies. The latter one dominates the energy output across the whole electro-magnetic spectrum. The results of our analyses are discussed in the framework of current blazar modeling.

**Key words.** $\gamma$ rays: observations – galaxies: active – galaxies: quasars: individual: 3C 454.3, CTA 102

## 1. Introduction

The Compton Gamma-Ray Observatory (CGRO), carrying four individual $\gamma$-ray experiments (EGRET, COMPTEL, OSSE, BATSE), explored the $\gamma$-ray sky for more than 9 years between April 1991 and June 2000. Due to the improved sensitivities, the wide field-of-view of the instruments and the long mission/exposure time, many new $\gamma$-ray sources were detected. For example, the EGRET telescope, sensitive to photon energies between 30 MeV and ~10 GeV, detected ~90 blazar-type Active Galactic Nuclei (AGN) (Hartman et al. 1999). These sources are characterized by a compact and radio-loud core, a flat radio spectrum ($S \propto \nu^{\alpha}$, $\alpha > -0.5$), and high flux variability at all energy bands. Among them are the quasars 3C 454.3 and CTA 102, which were discovered to be $\gamma$-ray emitters during the early CGRO mission in 1991 and 1992 (Nolan et al. 1993; Hartman et al. 1993). Both blazars were also detected in soft $\gamma$-rays and hard X-rays by the CGRO experiments COMPTEL (0.75–30 MeV) and OSSE (0.05–10 MeV). 3C 454.3 ($l/b$:86.11°/−38.18°, $z = 0.859$) and CTA 102 ($l/b$: 77.44°/−38.58°, $z = 1.037$) are prominent radio sources both showing superluminal motion (Unwin et al. 1989; Baath 1987).

Both sources belong to the OVV (optically violently variable) class (Angel & Stockman 1980) and the HPQ (high

polarization quasars) class of quasars. The optical polarization can be as high as 11% for CTA 102 (Moore & Stockman 1981) and is on average 3% for 3C 454.3 (Wills et al. 1992).

At soft X-ray energies the sources show also typical blazar signs, i.e. flux variability and a power-law shaped spectrum of energy index ~0.6 for 3C 454.3 (Comastri et al. 1997). At hard X-rays, 3C 454.3 and CTA 102 were occasionally detected by OSSE at energies between 50 keV and 1 MeV, both showing flux variability (McNaron-Brown et al. 1995).

Blom et al. (1995) reported the COMPTEL MeV-detections of both sources during the early CGRO observations in 1991 and 1992. According to the third EGRET catalog (Hartman et al. 1999) both blazars are repeatedly detected by EGRET at energies above 100 MeV, though 3C 454.3 on average at a higher flux level than CTA 102.

To generally investigate the MeV properties of both sources, we have consistently analyzed/reanalyzed all COMPTEL data, applying the most recent analysis methods. This supersedes the work of Blom et al. (1995), who reported the COMPTEL results on 3C 454.3 and CTA 102 from observations in 1991 and 1992. The analyses were carried out by first reanalyzing the early mission data, and then extending to the complete COMPTEL data base. We describe the instrument and the data analysis procedure in Sect. 2,

**Table 1.** COMPTEL observational periods of 3C 454.3 and CTA 102 during the whole CGRO mission, where at least one of the two objects was within 30° of the pointing direction. The CGRO VPs, their time periods, prime observational targets, offset angles, effective exposures and the CGRO Phases are given.

| VP # | Date | Target | Offset angle | | Effective exposure (days) | | CGRO Phase |
|---|---|---|---|---|---|---|---|
| | | | 3C 454.3 | CTA 102 | 3C 454.3 | CTA 102 | |
| 19.0 | 23/01/92-06/02/92 | G 058-43 | 15° | 22° | 3.08 | 3.79 | Phase I |
| 26.0 | 23/04/92-28/04/92 | MRK 335 | 18° | 24° | 0.61 | 0.49 | |
| 28.0 | 07/05/92-14/05/92 | MRK 335 | 18° | 24° | 1.13 | 0.90 | |
| 37.0 | 20/08/92-27/08/92 | MRK 335 | 15° | 21° | 1.23 | 1.01 | |
| 320.0 | 08/03/94-15/03/94 | NGC 7469 | 8° | 8° | 2.16 | 2.14 | Phase III |
| 327.0 | 17/05/94-24/05/94 | Gal 083-50 | 12° | 12° | 1.54 | 1.54 | |
| 336.0 | 01/08/94-04/08/94 | Gal 088-47 | 9° | 11° | 0.96 | 0.90 | |
| 410.0 | 24/01/95-14/02/95 | Gal 82-33 | 6° | 7° | 4.97 | 4.91 | Phase IV |
| 429.5 | 27/09/95-03/10/95 | GRO J2058+42 | 26° | 27° | 1.04 | 0.98 | |
| 507.0 | 28/11/95-07/12/95 | CTA 102 | 7° | 0° | 2.16 | 2.49 | Phase V |
| 507.5 | 07/12/95-14/12/95 | CTA 102 | 7° | 0° | 1.68 | 1.94 | |
| 514.0 | 13/02/96-20/02/96 | Gal 60-60 | 27° | 24° | 1.08 | 1.22 | |
| 601.1 | 15/10/96-29/10/96 | PSR J2043+2740 | 31° | 28° | 1.88 | 2.12 | Phase VI |
| 623.5 | 15/07/97-22/07/97 | Bl Lac | 28° | 31° | 1.06 | 0.92 | |
| 713.0 | 24/02/98-10/03/98 | Gal 110-20 | 24° | 30° | 2.61 | 1.97 | Phase VII |

the CGRO observations in Sect. 3, give the results and their discussion in Sects. 4 and 5, and finally conclude in Sect. 6.

## 2. Instrument and data analysis

The imaging Compton Telescope COMPTEL was sensitive to γ-rays in the energy range 0.75–30 MeV with an energy-dependent energy and angular resolution of 5%–8% (*FWHM*) and 1.7°–4.4°(*FWHM*), respectively. It had a large field of view of about 1 steradian and was able to detect γ-ray sources with location accuracy of the order of 1°–2°, depending on source flux. For the details about COMPTEL see Schönfelder et al. (1993).

COMPTEL contained two detector arrays in which an incident γ-ray photon is first Compton scattered in a detector of the upper detector array and – in the favorable case – then interacts with a detector of the lower detector array. The scattered photon direction $(\chi, \psi)$ is obtained from the interaction locations in the two detectors. The Compton scatter angle $\bar{\varphi}$ is calculated from the measured energy deposits of the photon in the two detectors. These quantities, scatter direction and angle, constitute a three-dimensional data space in which the spatial response of the instrument is cone-shaped and standard imaging methods, e.g. maximum entropy and maximum likelihood, are applied. In the COMPTEL data analysis package the maximum-likelihood method is used to estimate source parameters like detection significances, fluxes and flux errors. The detection significance is calculated from the quantity $-2\ln\lambda$, where $\lambda$ is the ratio of the likelihood $L_0$ (background) and the likelihood $L_1$ (source + background). The quantity $-2\ln\lambda$ has a $\chi_3^2$ distribution (3 degrees of freedom) for a unknown source and a $\chi_1^2$ distribution for a known source (de Boer et al. 1992). The instrumental COMPTEL background was modelled by the

standard filter technique in data space (Bloemen et al. 1994). Due to the high galactic-latitude location of the sources, no diffuse emission models were included in the analysis. To estimate the source flux, we applied instrumental point spread functions assuming an $E^{-2}$ power law shape for the source input spectrum. We note that the derived fluxes are weakly dependent on this particular shape. 3C 454.3 and CTA 102 are neighboring sources within the COMPTEL field-of-view and therefore their fluxes were estimated by simultaneous flux fits.

## 3. Observations

During the complete CGRO mission from April 1991 to June 2000, in 15 observational periods – so-called CGRO viewing periods (VPs), each lasting for typically 1 to 2 weeks – the offset angles (angle between the source position and the pointing direction of COMPTEL) were less than 30 degrees for either 3C 454.3 or CTA 102. Table 1 shows, that these 15 VPs are grouped within 6 so-called CGRO Phases. A CGRO Phase covers a time period of roughly 1 year. The whole CGRO mission was subdivided into 9 Phases, and COMPTEL observations on the two blazars are available up to Phase 7 in 1998. These 15 VPs add up to total effective exposures (100% COMPTEL pointed directly to the source) of 27.19 days for 3C 454.3 and 27.32 days for CTA 102.

## 4. Results

### 4.1. Reanalysis of early-mission data

During the COMPTEL mission, the data analysis methods (e.g. background modeling, event selections) were improved compared to the earlier Phases. We reanalyzed the
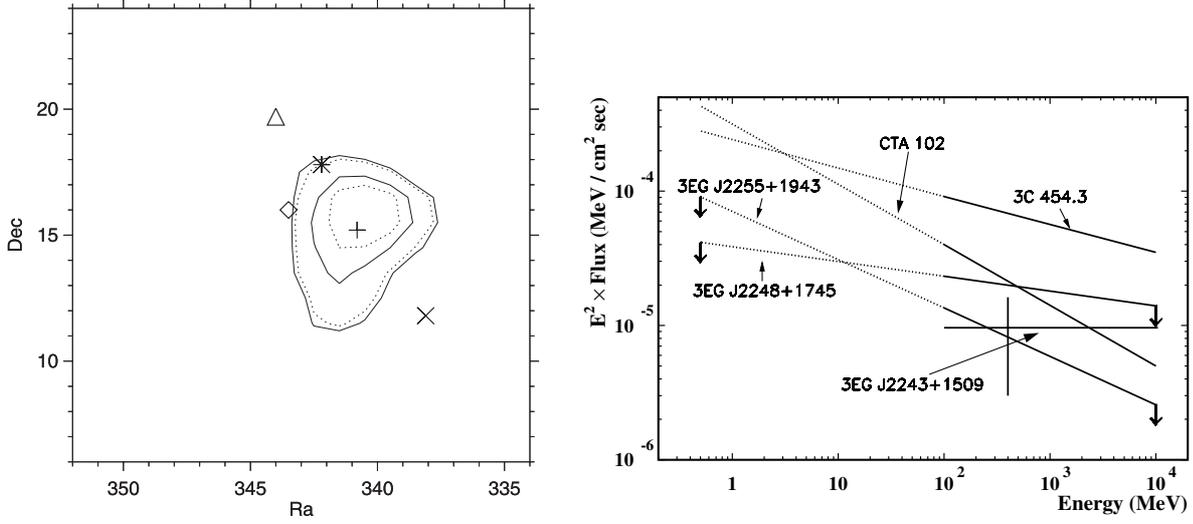
**Fig. 1.** *Left*: COMPTEL 10-30 MeV significance (solid contours) and error location (dotted contours) map of the 3C 454.3 (⋄) and CTA 102 (×) sky region for CGRO Phase 1 (May 1991 to November 1992). The locations of three nearby EGRET sources 3EG J2243+1509 (+), 3EG J2248+1745 (∗), and 3EG J2255+1943 (△) in this sky region are overlaid. The significance contour lines start at $3\sigma$ (outer solid contour) with steps of $0.5\sigma$, and the error location contour lines at $1\sigma$ (inner dotted contour) with steps of $1\sigma$. *Right*: best-fit spectral shapes in the EGRET band (solid lines) and their spectral extrapolations throughout the COMPTEL band (dotted lines) are shown for 4 of the 5 EGRET sources of the map, according to the source parameters given in the third EGRET catalog (Hartman et al. 1999) for CGRO Phase 1 (P1). These shapes are generated by using the simultaneously (P1) measured flux values and the given (non-simultaneous) spectral indices for P1234. Note that the spectral shapes for 3EG J2255+1943 and 3EG J2248+1745 are upper limits. For 3EG J2243+1509 the third EGRET catalog does not provide a spectral shape. In order to estimate its contribution, we plot its simultaneous flux value at an assumed center of energy of 400 MeV. 3C 454.3 and CTA 102 should be the strongest MeV sources.

**Table 2.** Fluxes and upper limits of 3C 454.3, CTA 102 and the unidentified EGRET source 3EG J2255+1943 for different observational periods in units of $10^{-5}$ ph cm$^{-2}$ s$^{-1}$. The errors are $1\sigma$ and the upper limits are $2\sigma$. An upper limit is given when the significance of an individual flux value is less than $1\sigma$.

| Energy | 3C 454.3 | | | CTA 102 | | | 3EG J2255+1943 | |
|---|---|---|---|---|---|---|---|---|
| (MeV) | Phase 1 | Phases 1−4 | Phases 1−7 | Phase 1 | Phases 1−4 | Phases 1−7 | Phases 1−4 | Phases 1−7 |
| 0.75–1 | <8.35 | <6.05 | <4.79 | <8.48 | <7.56 | <7.40 | <7.6 | <6.1 |
| 1–3 | <8.58 | $6.40 \pm 2.78$ | $5.59 \pm 2.30$ | $5.03 \pm 4.03$ | $4.26 \pm 2.80$ | <4.64 | <6.73 | <5.49 |
| 3–10 | $2.96 \pm 1.85$ | $3.94 \pm 1.16$ | $3.95 \pm 0.95$ | <5.26 | <2.92 | <2.83 | <2.73 | <2.2 |
| 10–30 | $1.74 \pm 0.69$ | $0.60 \pm 0.43$ | $0.45 \pm 0.34$ | $1.12 \pm 0.64$ | $0.88 \pm 0.38$ | $0.64 \pm 0.31$ | $1.03 \pm 0.41$ | $0.70 \pm 0.34$ |

early-mission data, published by Blom et al. (1995), using the most up-to-date methods. Our results are generally consistent with those published by Blom et al. (1995). We find a significant excess in the uppermost (10−30 MeV) COMPTEL band, which is consistent with the locations of 3C 454.3 and CTA 102 (Fig. 1). However, EGRET has detected three more γ-ray sources in this sky region (Hartman et al. 1999): 3EG J2255+1943 ($\alpha, \delta$ = 343.99°,19.73°; tentatively identified with the blazar PKS 2250+1926), 3EG J2243+1509 ($\alpha, \delta$ = 340.78°,15.17°; unidentified), and 3EG J2248+1745 ($\alpha, \delta$ = 342.24°,17.77°; unidentified). They are also positionally consistent with this MeV emission (Fig. 1). Due to the poorer angular resolution of COMPTEL compared to EGRET, these five known EGRET sources cannot be resolved by COMPTEL. In order to elaborate on this MeV excess, we considered the time behaviour of these 5 sources as observed by EGRET. According to the third EGRET catalog (Hartman et al. 1999), 3EG 2255+1943 was not detected in any of these

early-mission VPs, and therefore we consider its contribution to this 10−30 MeV excess as negligible. 3EG J2243+1509 was only detected in VP 26 (~$4\sigma$ level), and 3EG J2248+1745 only in VP 28 (~$3\sigma$ level). In contrast, 3C 454.3 and CTA 102 were detected in all of these early VPs. For the sum of the four VPs in Phase 1, the third EGRET catalog lists the following fluxes (units $10^{-8}$ cm$^{-2}$ s$^{-1}$): $75.0 \pm 6.8$ for 3C 454.3, $27.7 \pm 4.5$ for CTA 102, <9.9 for 3EG J2255+1943, $9.7 \pm 4.7$ for 3EG J2243+1509, and <20.8 for 3EG J2248+1745. The extrapolations of the averaged spectra to MeV energies show that 3C 454.3 and CTA 102 should have the strongest MeV emission (Fig. 1). Therefore we assume that the majority of the detected MeV emission should be due to 3C 454.3 and CTA 102, because they are the strongest EGRET sources during this time period.

To test our assumption, we first analyzed the four VPs individually. The results are not conclusive because in individual VPs the MeV emission is too weak to be attributed to
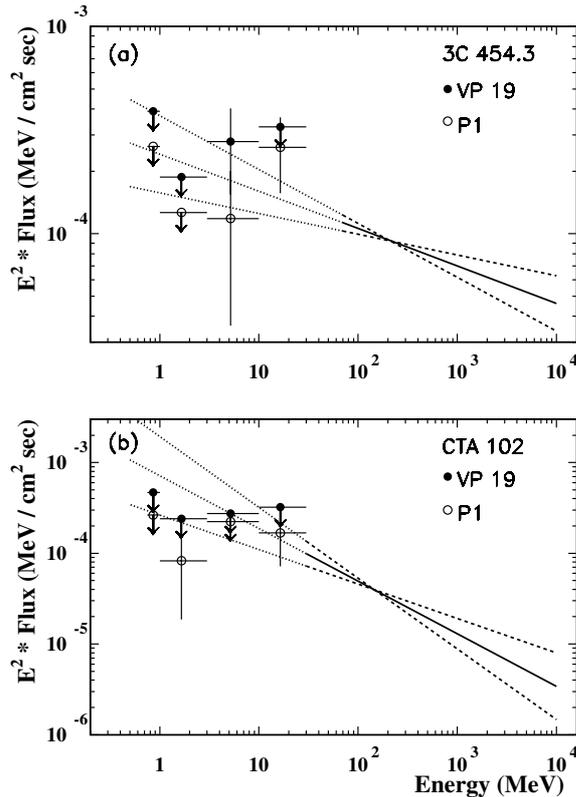
**Fig. 2.** Combined COMPTEL/EGRET spectra of 3C 454.3 **a)** and CTA 102 **b)**. The COMPTEL data are from complete CGRO Phase 1 (open circles) and VP 19 (filled circles). The error bars are $1\sigma$ and the upper limits are $2\sigma$. The EGRET spectra are from VP 19. The solid lines represent the best-fit EGRET spectra, the dashed lines their $1$-$\sigma$ error limits in slope, and the dotted lines their extrapolations towards MeV energies.

individual sources. Then we analyzed separately the combinations of VPs 19, 28, 37 (3EG J2243+1509 not detected by EGRET), VPs 19, 26, 37 (3EG J2248+1745 not detected by EGRET), and VP 19, 37 (only 3C 454.3 and CTA 102 detected by EGRET). In all cases an MeV excess remains, though accordingly reduced in significance. The 3C 454.3 and CTA 102 fluxes, obtained from the sum of the 4 VPs (Table 2), are consistent with those from only VPs 19+37 within error bars. Analyzing the sum of the four VPs by assuming 3C 454.3 and CTA 102 as the only emitting sources and removing their contributions from the map, provides a rather empty COMPTEL map with some remaining emission from the location of 3EG J2243+1509.

In summary, the excess is consistent with the main contributions being from 3C 454.3 and CTA 102, although this cannot be finally proven due to the insufficient angular resolution of COMPTEL. Their flux estimate is uncertain by the probable minor contributions of the two unidentified sources in VP 26 and 28.

The simultaneous COMPTEL/EGRET spectra of 3C 454.3 and CTA 102 of VP 19 are shown in Fig. 2. The EGRET spectral shapes are from Hartman et al. (1993) for 3C 454.3 and from Nolan et al. (1993) for CTA 102. The COMPTEL spectral data are consistent with the extrapolations of the EGRET

spectra. If the COMPTEL spectral points of the 4 VPs are combined with the EGRET spectra for VP 19 (the only ones publicly available), the 10−30 MeV flux points are again consistent with the extrapolations of the EGRET spectra, supporting our interpretation that 3C 454.3 and CTA 102 are the main emitting sources in Fig. 1. The spectra show the trend of a flattening at MeV energies for both sources (Fig. 2).

### 4.2. Complete mission

### 4.2.1. Detections

No source is significantly detected (threshold $3\sigma$) in this sky region in individual VPs in any of the four standard (0.75−1, 1−3, 3−10, 10−30 MeV) COMPTEL bands. In order to improve the statistics, we combined the observations listed in Table 1 into 2 periods: CGRO Phases 1 to 4 (simultaneous to the third EGRET catalog) and the sum of all data, i.e. the complete COMPTEL coverage of this sky region during the CGRO mission. This results in skymaps showing significant MeV emission above 3 MeV from this sky region.

The 10−30 MeV maps (Fig. 3) show emission peaks of $\sim4.5\sigma$ (Phases 1 to 4) and $\sim3.9\sigma$ (all mission), located in between 3C 454.3 and CTA 102, now with extensions towards 3EG J2255+1943. Again, COMPTEL cannot resolve the 5 EGRET sources, and therefore we checked the EGRET measurements for this time period. Figure 4 shows the measured EGRET spectra/fluxes of the 5 sources time-averaged for the CGRO Phases 1 to 4. Because 3C 454.3 and CTA 102 are expected to be the brightest MeV emitters, we naturally consider both of them as prime candidates for this emission. For 3EG J2243+1509 is only an upper limit given in the third EGRET catalog (only detected in VP 26). Therefore we neglect its contribution to the MeV excess, although it is the source closest to the emission peak. The contributions from 3EG J2248+1745 and 3EG J2255+1943 to this 10−30 MeV excess are expected to be at the same level, although a factor of 5 to 10 below the expected contributions of 3C 454.3 and CTA 102. Therefore we would not expect much contribution from these sources. However, the maps of Fig. 3 suggest, by their extensions towards 3EG J2255+1943, a significant contribution of this source, whose EGRET spectral index for the P1234 time period, $2.36 \pm 0.61$, is rather uncertain (Hartman et al. 1999). As suggested by the maps and the coincidence in time (the extensions are consistent with the flaring of this source in VPs 336 and 410), we included 3EG J2255+1943 in the flux fitting procedure. The fluxes of three sources, 3C 454.3, CTA 102 and 3EG J2255+1943, are listed in Table 2 for the Phases 1−4 and Phases 1−7. They were obtained by a simultaneous three-source fit. The 10−30 MeV fluxes of CTA 102 are not dependent on the inclusion of 3EG J2255+1943 in the fitting procedure, while the flux values of 3C 454.3 vary within a factor of 2 with, however, overlapping error bars.

In the 3−10 MeV band, a significant excess of $\sim5.3\sigma$ (one degree of freedom) is detected in this sky region (Fig. 5) for the sum of all 15 VPs. Because only 3C 454.3 is located inside
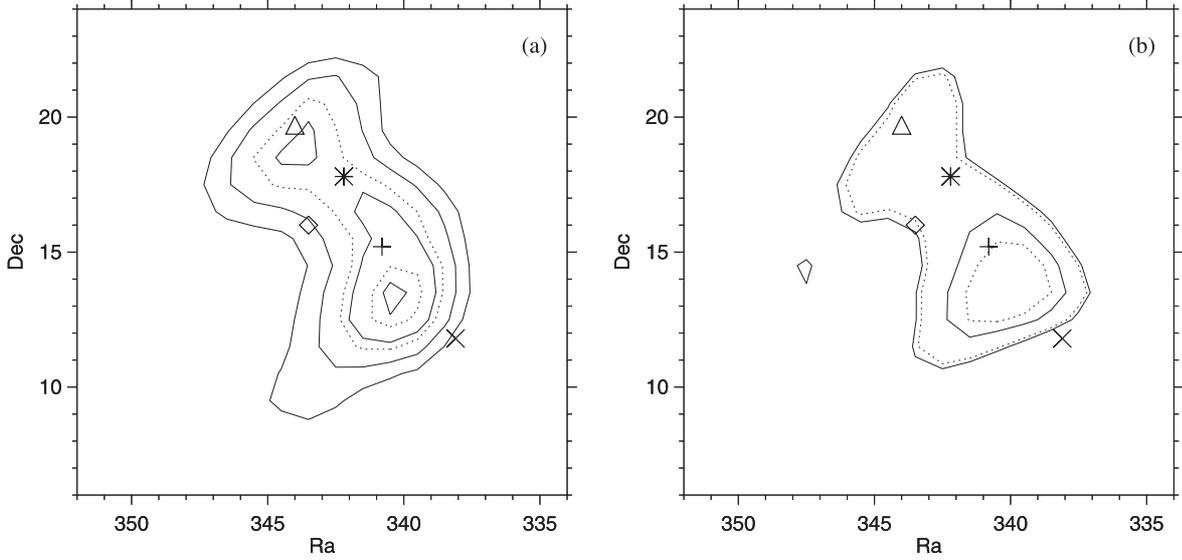
**Fig. 3.** COMPTEL 10−30 MeV significance (solid contours) and error location (dotted contours) map of the 3C 454.3 (⋄) and CTA 102 (×) sky region for **a)** CGRO Phase 1 to 4 (corresponding to P1234 in the third EGRET catalog), and **b)** the sum of all COMPTEL data. The locations of three nearby EGRET sources 3EG J2243+1509 (+), 3EG J2248+1745 (∗), and 3EG J2255+1943 (△) in this sky region are overlaid. The significance contour lines start at 3σ (outer solid contour) with steps of 0.5σ, and the error location contour lines at 1σ (inner dotted contour) with steps of 1σ.
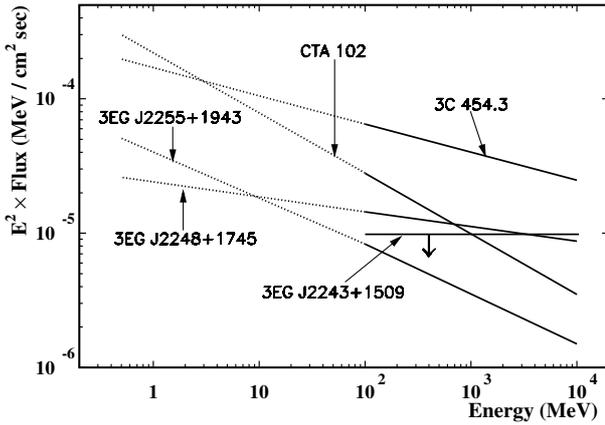


**Fig. 4.** Best-fit spectral shapes in the EGRET band (solid lines) and their spectral extrapolations throughout the COMPTEL band (dotted lines) are shown for 4 of the 5 EGRET sources of this sky region according to the source parameters given in the third EGRET catalog (Hartman et al. 1999). These shapes are generated by using the P1234 measured flux values and spectral indices. For 3EG J2243+1509 the third EGRET catalog does not provide a spectral shape. In order to estimate its contribution, we plot its P1234 upper flux limit at an assumed center of energy of 400 MeV. 3C 454.3 and CTA 102 should be the strongest MeV sources.

the 3σ error contour – 4.5σ detection significance at the actual source position – we attribute this emission solely to 3C 454.3.

### 4.2.2. Flux variability

A search for flux variability was carried out for 3C 454.3 and CTA 102 in the four standard energy bands using all individual VPs. All MeV light curves are statistically consistent with a constant flux for both sources during the analyzed period
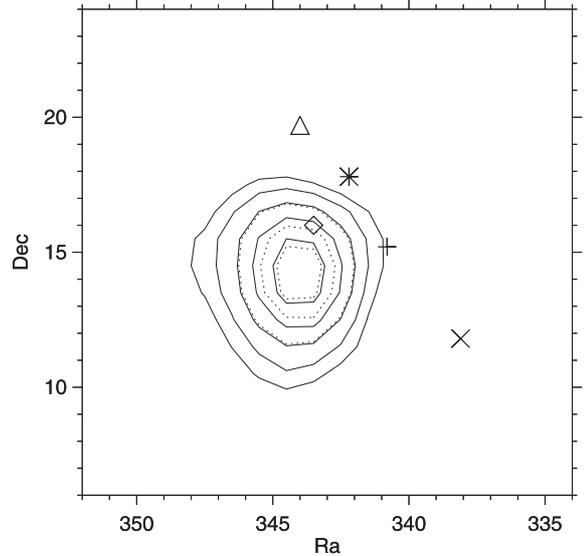


**Fig. 5.** COMPTEL 3−10 MeV significance (solid contours) and error location (dotted contours) map of the 3C 454.3 (⋄) and CTA 102 (×) sky region for the sum of all COMPTEL data. The locations of three other nearby EGRET sources, 3EG J2243+1509 (+), 3EG J2248+1745 (∗), and 3EG J2255+1943 (△), are overlaid. The significance contour lines start at 3σ (outer solid contour) with steps of 0.5σ, and the error location contour lines at 1σ (inner dotted contour) with steps of 1σ.

of 7 years, although flux variations were found in neighboring bands by OSSE (McNaron-Brown et al. 1995) and EGRET (Mukherjee et al. 1997) for both sources. The COMPTEL 10−30 MeV detections are weak for both sources. The trend is that COMPTEL detects the sources during the early mission (3C 454.3 in Phase I; CTA 102 in Phase I and III) at periods when EGRET reported flaring activity (Hartman et al. 1999).
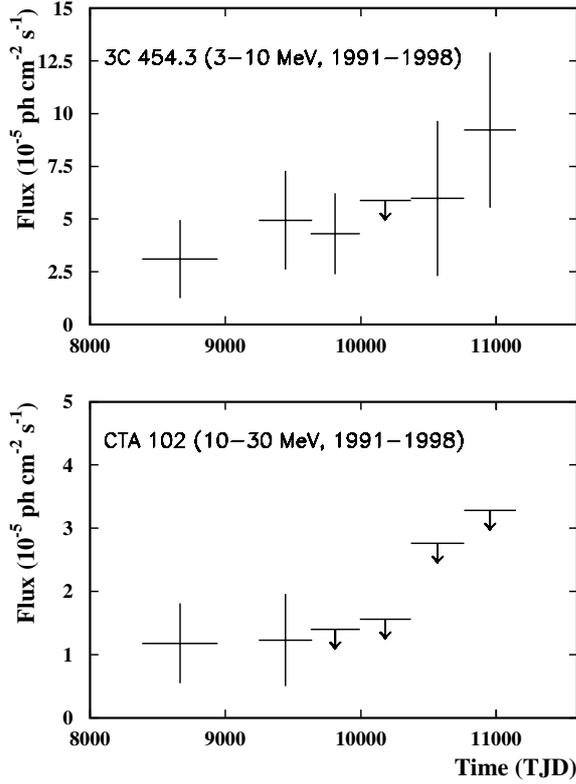
**Fig. 6.** The 3−10 MeV light curve of 3C 454.3 (*upper panel*) and the 10−30 MeV light curve of CTA 102 (*lower panel*) with each bin averaged over one CGRO Phase. Phase 2 is missing due to the lack of observations in this period. The error bars are 1σ and the upper limits are 2σ.

At later periods only non-detections are derived. In contrast to CTA 102 we find significant evidence for 3C 454.3 in the sum of the COMPTEL 3−10 MeV data. Subdividing this emission into time bins according to the CGRO phase, indicates a weak (near the detection threshold of COMPTEL) but likely stable MeV emission (Fig. 6). This is consistent with the significant detection in the sum of all data, and the non-detections in individual VPs.

### 4.2.3. Energy spectra

To further investigate the MeV properties of both blazars, we generated MeV spectra for different time periods. The time-averaged ones, containing all COMPTEL mission data, are shown in Fig. 7. The spectrum of 3C 454.3 indicates a power maximum (at least with respect to MeV energies) in the 3−10 MeV band. No conclusion can be drawn from the spectrum of CTA 102 because only the 10−30 MeV band yields a weak detection. To combine the COMPTEL and EGRET spectra simultaneously (Fig. 8), we generated time-averaged COMPTEL spectra for the CGRO Phases 1−4, covering the time period of the third EGRET catalog. The COMPTEL data points are consistent with the EGRET spectral extrapolations within the 1 sigma error limits in photon index although they show the trend of a spectral turnover. To verify this trend, we added non-simultaneous published (McNaron-Brown et al. 1995) OSSE data, measured for both
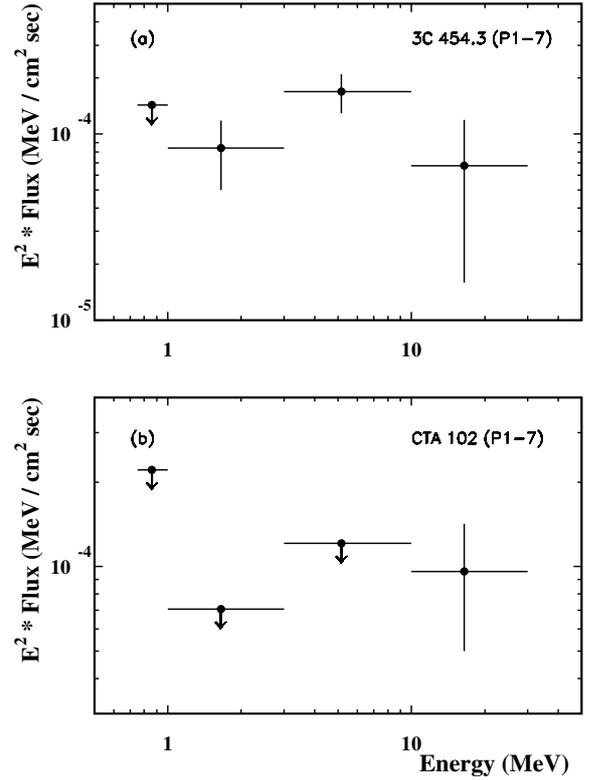


**Fig. 7.** The COMPTEL spectra of 3C 454.3 **a)** and CTA 102 **b)** for the sum of all COMPTEL data. The error bars are 1σ and the upper limits are 2σ.

sources in 1994 (VPs 317, 319, 319.5 and 323 for 3C 454.3; VPs 316, 317 and 323 for CTA 102). These combined OSSE/COMPTEL/EGRET spectra show clearly the spectral turnover with a power maximum in the COMPTEL range for both sources (Fig. 9). OSSE measured a photon index of $1.5^{+0.6}_{-0.4}$ for 3C 454.3 in VP 317, while EGRET reports a time-averaged spectral index of 2.21 ± 0.06 (Hartman et al. 1999). For CTA 102, OSSE observed a photon index of $1.0^{+0.7}_{-0.6}$ in VP 323 (McNaron-Brown et al. 1995), while the third EGRET catalog reports a time-averaged spectral index of 2.45 ± 0.14. Therefore the changes in spectral index from high energy γ-rays to hard X-rays, at least for CTA 102, have to be larger than 0.5.

In order to obtain a view on the general – radio to γ-rays – radiation behaviour of both blazars, we supplemented these CGRO γ-ray data by published (non-simultaneous) measurements at lower energies (Fig. 10). The two multifrequency spectra are generally similar, both showing two spectral maxima. The low-energy ones are in the IR-band, while the high-energy ones, dominating the source luminosity, are at MeV-energies.

## 5. Discussion

Our analyses on the combined COMPTEL data from 1991 to 1998 show weak detections of 3C 454.3 and CTA 102 at energies above 10 MeV, and a significant detection of 3C 454.3 in the 3−10 MeV band. The time-averaged MeV spectra are consistent with the extrapolations of the EGRET spectra (Fig. 8),
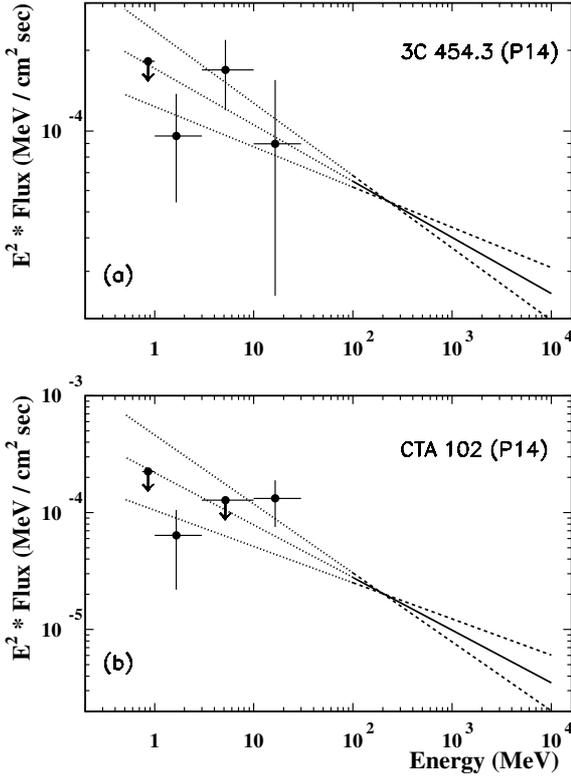
**Fig. 8.** Simultaneous COMPTEL and EGRET spectra of 3C 454.3 **a)** and CTA 102 **b)** for the CGRO Phases 1 to 4. The filled circles represent the COMPTEL spectral points. The solid lines represent the best-fit EGRET spectra, the dashed lines their 1-$\sigma$ error limits in slope, and the dotted lines the extrapolations into the COMPTEL band.

**Fig. 9.** Non-simultaneous OSSE, COMPTEL and EGRET γ-ray spectra of 3C 454.3 **a)** and CTA 102 **b)**. The solid lines represent the EGRET spectra inside the 1$\sigma$ error limits in slope. The OSSE results (McNaron-Brown et al. 1995) are from 4 VPs in 1994 for 3C 454.3, and from 3 VPs in 1994 for CTA 102 (see text). The EGRET spectra (Hartman et al. 1999) are from the first 4 CGRO Phases, i.e. time-averaged between April 1991 and October 1995.

while the addition of the OSSE hard X-ray data reveal for both sources a significant spectral turnover with a power maximum at lower MeV energies (Fig. 9). Assuming a Friedmann universe, $H_0 = 75$ km s$^{-1}$ Mpc$^{-1}$ and $q_0 = 0.5$, we derive isotropic luminosities of $1.6 \times 10^{48}$ erg s$^{-1}$ and $7.5 \times 10^{47}$ erg s$^{-1}$ for 3C 454.3 (above 3 MeV) and CTA 102 (above 10 MeV), respectively. The corresponding minimum mass of the central black holes by assuming Eddington-limited accretion are $1.1 \times 10^{10}$ $M_\odot$ (3C 454.3) and $5.5 \times 10^9$ $M_\odot$ (CTA 102) in the Thompson regime. These values decrease to $2.85 \times 10^8$ $M_\odot$ and $8 \times 10^7$ $M_\odot$ in the Klein-Nishina regime. From OSSE variability measurements in 1995, McNaron-Brown et al. (1995) derive upper mass limits for the central black holes of $5.6 \times 10^{10}$ $M_\odot$ for 3C 454.3 and $8.9 \times 10^{10}$ $M_\odot$ for CTA 102.

Short-term variability together with high luminosities are two main characteristics of EGRET-detected γ-ray blazars. Both facts together require a small photon-dense emission region. However, for several blazars – among them 3C 454.3 and CTA 102 (McNaron-Brown et al. 1995) – the derived high photon densities imply the pair production optical depth $\tau_{\gamma\gamma}$ to be larger than 1, which would lead to a cut-off of the γ-ray spectrum. To avoid this contradiction, beaming of the photons is generally assumed. Therefore current models for the γ-ray emission in blazars were developed in a beaming scenario, which generally assumes that the γ-ray emission is produced through inverse-Compton (IC) scattering of photons off
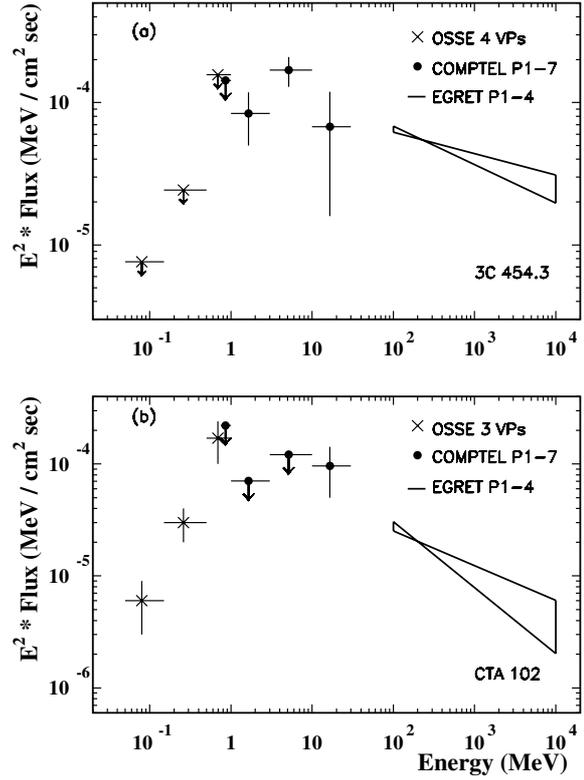
relativistic particles in a plasma jet whose orientation is close to our line of sight.

The primary accelerated jet particles can be either electrons or protons. Both are successful in interpreting the spectral energy distribution (SED) of blazars of different types, like flat-spectrum radio quasars (FSRQs) or BL Lac objects. 3C 454.3 and CTA 102 belong to the FSRQ-class of blazars. A typical property of blazars is a two-hump spectrum with low-energy peaks from infrared to X-ray energies and high-energy peaks from MeV up to TeV energies. Such spectra are usually interpreted as synchrotron and inverse-Compton (IC) emission from a relativistic jet. In a leptonic scenario, the IC models can be categorized according to the origin of the soft photons into synchrotron-self Compton (SSC) models (the self-generated synchrotron photons are the target photons of the relativistic jet leptons, e.g. Maraschi et al. 1992; Bloom & Marscher 1996) and so-called external Compton (EC) models (the soft target photons originate from outside the jet, e.g. Dermer & Schlickeiser 1993; Sikora et al. 1994; Blandford & Levinson 1995). In pure SSC models, the high-energy peak relates to the low-energy one by $\nu_C \propto \langle \gamma^2 \rangle \nu_S$, where $\nu_S$ is the frequency of the synchrotron peak, $\nu_C$ the frequency of the SSC peak, and $\langle \gamma \rangle$ the average Lorentz-factor (energy) of the electrons. In a SSC scenario, $\gamma$ should be in the range of $10^3$–$10^5$ for 3C 454.3 and CTA 102 according to the peak
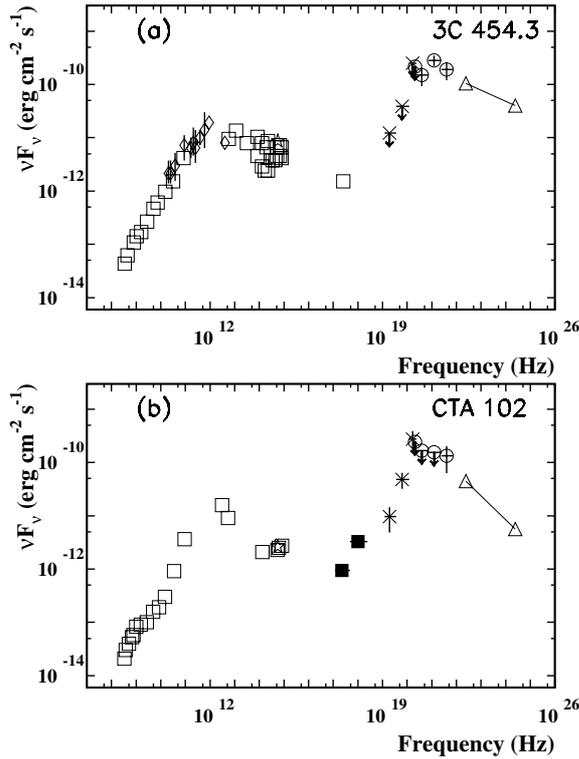
**Fig. 10.** Non-simultaneous SEDs of 3C 454.3 **a)** and CTA 102 **b)**. The solid lines with triangles on each end represent the time-averaged (Phase 1–4) EGRET spectra (Hartman et al. 1999), open circles the COMPTEL measurements (all mission), "∗" the OSSE observations in 1994 (McNaron-Brown et al. 1995), and filled squares the ASCA measurements in 1995 (taken from NED). The low-energy data symbolized by open diamonds are taken from Montigny et al. (1995), and the ones symbolized by open squares from Impey et al. (1988).
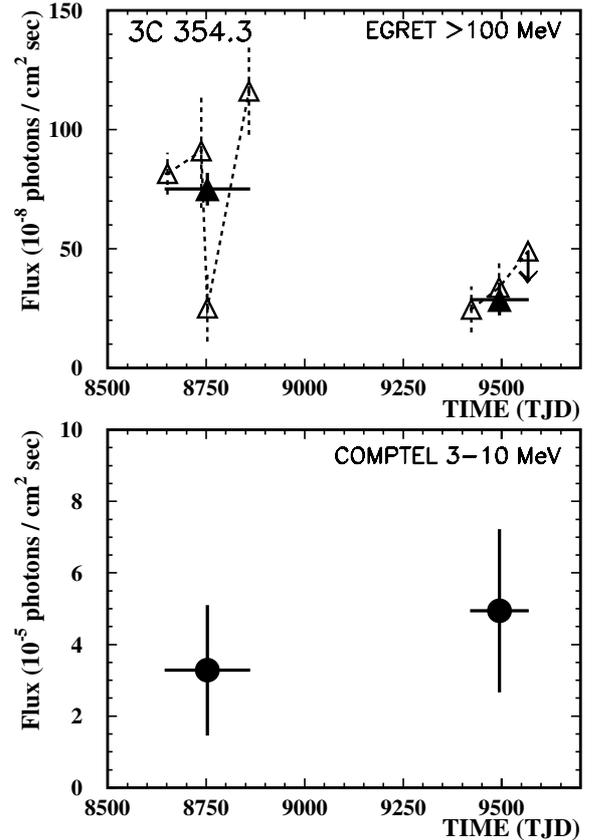


**Fig. 11.** Simultaneous EGRET (>100 MeV; △) and COMPTEL (3–10 MeV; circles) flux measurements of 3C 454.3. The filled triangles represent the average EGRET fluxes of CGRO Phase 1 and 3 (Hartman et al. 1999), while the open triangles the fluxes as measured in individual VPs. The obvious and significant flux decline (factor of ~3) at energies above 100 MeV from Phase 1 (in 1992) to Phase 3 (in 1994) has no counterpart at COMPTEL energies, indicating an independent variability behaviour at the two bands. The error bars are 1σ.

positions in their SEDs (Fig. 10). The EC process is always taken into account in modeling the $\gamma$-ray flaring behaviour of blazars, due to its stronger dependence on the bulk Lorentz factor. The SEDs of the flaring $\gamma$-ray blazars PKS 0528+134, 3C 273 and 3C 279 are well interpreted in such a multi-component scenario (e.g. Mukherjee et al. 1999; Collmar et al. 2000; Hartman et al. 2001). However, according to the investigations on PKS 0528+134 by Mukherjee et al. (1999) and on 3C 279 by Hartman et al. (2001), the contribution of the EC process is also important if the blazar is in a low $\gamma$-ray state. Furthermore, Sambruna et al. (1997) found that the EC scattering may be the primary cooling mechanism in the low $\gamma$-ray state of PKS 0528+134, if the $\gamma$-ray flux exceeds the optical one.

Ghisellini et al. (1998) modeled the SEDs of 51 $\gamma$-ray blazars with similar SEDs as in Fig. 10 (among them 3C 454.3 and CTA 102) by two types of models: a pure SSC model and a combined SSC/EC model. They assumed a black body distribution for the soft EC photons, which are radiated from an optically thick accretion disk. They found that for most blazars the SED can in principle be represented by both types of models. They suggest that the sequence *high frequency peaked BL Lac object → low frequency peaked BL Lac object → flat-spectrum radio quasars* (HBL→LBL→FSRQs) may be related

to an increasing dominance of the EC over the SSC emission. Ghisellini et al. (1998) note that the bulk Lorentz factor, $\Gamma$, has to be of the order of 10–15 to produce a power maximum peaking at MeV energies. In EC models the IC target photons can be the direct accretions disk photons (ECD; e.g. Dermer et al. 1992; Dermer & Schlickeiser 1993), the disk photons reflected by the broad-line region (ECC; e.g. Sikora et al. 1994) and the synchrotron photons reflected by the broad-line region (Rsy; e.g., Ghisellini & Madau 1996). In the modeling of PKS 0528+134 (Mukherjee et al. 1999) and 3C 279 (Hartman et al. 2001) a bulk Lorentz factor strength between ~5 and ~20 is found, which leads to a narrow ECD emission component sticking out at MeV energies on top of a broad SSC component.

The most interesting new result is the evidence for a longterm steady emission of 3C 454.3 in the COMPTEL 3–10 MeV band, which – at least on time average – covers the IC peak of the blazar emission. Interpreting our data in the framework of leptonic multicomponent models, we attribute this MeV emission to an ECD component on top of an SSC component, given the high bulk Lorentz factor derived by Ghisellini et al. (1998) for 3C 454.3. This rather

stable MeV emission does not agree with the time variability observed by EGRET at energies above 100 MeV (Fig. 11). While at EGRET energies the flux level decreased by a factor of ~3 (Hartman et al. 1999), the COMPTEL 3−10 MeV flux level stays the same. These different variability behaviours probably suggest that different emission processes are at work in these two energy bands. Such a behaviour is consistent with the multicomponent modeling of 3C 279 by Hartman et al. (2001). In this framework, we would attribute the EGRET part of the spectrum to the ECC component, while, as already mentioned above, the COMPTEL part to the ECD component. In any case, between Phase 1 and Phase 3 something has changed inside 3C 454.3, which leaves the MeV emission unaffected, while significantly changing the flux at energies above 100 MeV. Due to the different dependence of the ECD and ECC on the bulk Lorentz factor $\Gamma$ (Böttcher 1999), this peculiar variability behaviour could reflect a reduction in $\Gamma$ from Phase 1 to Phase 3.

This uncorrelated variability behaviour is similar to the one observed in 3C 273 (Collmar et al. 2000), where during a two-week flaring event at EGRET energies, the MeV-flux at COMPTEL energies did not follow this high-energy flare. Apart from the different time-scales, these two observations are quite similar. Also in other respects, 3C 454.3 has similar MeV properties as 3C 273. Both blazars seem to have a rather stable MeV emission over years, and a clear spectral maximum in the 3−10 MeV band (Collmar et al. 2001). This probably suggests that the same physical processes are responsible for their MeV radiation.

## 6. Conclusion

We report the results of an analysis of all COMPTEL data of the γ-ray blazars 3C 454.3 and CTA 102. Our results of the early mission (Phase 1) are consistent with the ones of Blom et al. (1995). We conclude that the observed excess in the 10−30 MeV band during this early period, located in between the two blazars, is dominated by 3C 454.3 and CTA 102, but might have some minor contributions from nearby unidentified EGRET γ-ray sources. In the time-averaged (Phase 1 to 4 and Phase 1 to 7) data, we obtain significant MeV emission in the uppermost (10−30 MeV) COMPTEL band, which we attribute to 3C 454.3, CTA 102 and 3EG J2255+1943. We find a strong detection of 3C 454.3 in the 3−10 MeV band. Time-resolved analyses suggest a likely steady (although near the COMPTEL threshold) MeV emission from 3C 454.3 in the 3−10 MeV band, which yields the strong detection in the sum of all COMPTEL data. This likely steady MeV emission is different to the significantly observed time variability at EGRET energies. Given this fact, we conclude that different emission mechanisms dominate at these energy bands. According to current leptonic multicomponent emission scenarios, this may be the Comptonization of direct accretion disk photons at COMPTEL energies, and at EGRET energies the Comptonization of accretion disk photons which have been scattered into the jet region by the broad-line region clouds.

The MeV spectra of both sources are consistent with the spectral extrapolations of the contemporaneous EGRET spectra. However, the inclusion of (non-simultaneous) OSSE data reveals a strong spectral turnover at MeV energies. Putting the COMPTEL data into multifrequency perspective reveals that – at least on time average – the peak of the IC emission, which dominates the luminosity, is for both sources at MeV energies.

## References

Angel, J. R. P., & Stockman, H. S. 1980, ARA&A, 8, 321
Baath, L. B. 1987, in Superluminal Radio Sources, ed. J. A. Zensus, & T. J. Pearson (Cambridge: Cambridge University Press), 206
Blandford, R., & Levinson, A. 1995, ApJ, 441, 79
Bloemen, H., Hermsen, W., Swanenburg, B. N., et al. 1994, ApJS, 92, 419
Blom, J. J., Bloemen, H., Bennett, K., et al. 1995, A&A, 295, 330
Bloom, S. D., & Marscher, A. P. 1996, ApJ, 461, 657
de Boer, H., Bennett, K., Bloemen, H., et al. 1992, in Data Analysis in Astronomy IV, ed. V. Di Gesù, L. Scarsi, R. Buccheri, et al. (New York: plenum Press), 241
Böttcher, M. 1999, AIP Conf. Proc., 515, 31
Collmar, W., Reimer, O., Bennett, K., et al. 2000, A&A, 354, 513
Collmar, W., Schönfelder, V., Zhang, S., et al. 2001, in Proceedings of the γ-Ray Astrophysics 2001, ed. S. Ritz, N. Gehrels, & C. R. Shrader, New York, AIP Conf. Proc., 587, 271
Comastri, A., Fossati, G., Ghisellini, G., & Molendi, S. 1997, ApJ, 480, 534
Dermer, C. D., Schlickeiser, R., & Mastichiadis, A. 1992, A&A, 256, L27
Dermer, C. D., & Schlickeiser, R. 1993, ApJ, 416, 458
Ghisellini, G., & Madau, P. 1996, MNRAS, 280, 67
Ghisellini, G., Celotti, A., Fossati, G., Maraschi, L., & Comastri, A. 1998, MNRAS, 301, 451
Hartman, R. C., Bertsch, D. L., Dingus, B. L., et al. 1993, ApJ, 407, L4
Hartman, R. C., Bertsch, D. L., Bloom, S. D., et al. 1999, ApJS, 123, 79
Hartman, R. C., Böttcher, M., Aldering, G., et al. 2001, ApJ, 553, 683
Impey, C. D., & Neugebauer, G. 1988, ApJ, 95, 307
Maraschi, L., Ghisellini, G., & Celotti, A. 1992, ApJ, 397, L5
McNaron-Brown, K., Johnson, W., Jung, G. V., et al. 1995, ApJ, 451, 575
von Montigny, C., Bertsch, D. L., Chiang, J., et al. 1995, ApJ, 440, 525
Moore, R. L., & Stockman, H. S. 1981, ApJ, 243, 60
Mukherjee, R., Bertsch, D. L., Bloom, S. D., et al. 1997, ApJ, 490, 116
Mukherjee, R., Böttcher, M., Hartman, R. C., et al. 1999, ApJ, 527, 132
Nolan, P. L., Bertsch, D. L., Fichtel, C. E., et al. 1993, ApJ, 414, 82
Sambruna, R. M., Urry, C. M., & Maraschi, L. 1997, ApJ, 474, 639
Schönfelder, V., Aarts, H., Bennett, K., et al. 1993, ApJS, 86, 657
Sikora, M., Begelman, M. C., & Rees, M. J. 1994, ApJ, 421, 153
Unwin, S. C., Cohen, M. H., Hodges, M. W., Zensus, J. A., & Biretta, J. A. 1989, ApJ, 340, 117
Wills, B. J., et al. 1992, ApJ, 398, 464